Stem Cell Reports
Article

ISSCR

OPEN ACCESS

Enhanced Dentate Neurogenesis after Brain Injury Undermines Long-Term Neurogenic Potential and Promotes Seizure Susceptibility

Eric J. Neuberger,[1] Bogumila Swietek,[1] Lucas Corrubia,[1] Anagha Prasanna,[1] and Vijayalakshmi Santhakumar[1,*]

[1]Department of Pharmacology, Physiology & Neuroscience, Rutgers New Jersey Medical School, Rutgers Biomedical & Health Sciences, MSB-H-512, 185 S. Orange Ave., Newark, NJ 07103, USA

*Correspondence: santhavi@njms.rutgers.edu

http://dx.doi.org/10.1016/j.stemcr.2017.07.015

SUMMARY

Hippocampal dentate gyrus is a focus of enhanced neurogenesis and excitability after traumatic brain injury. Increased neurogenesis has been proposed to aid repair of the injured network. Our data show that an early increase in neurogenesis after fluid percussion concussive brain injury is transient and is followed by a persistent decrease compared with age-matched controls. Post-injury changes in neurogenesis paralleled changes in neural precursor cell proliferation and resulted in a long-term decline in neurogenic capacity. Targeted pharmacology to restore post-injury neurogenesis to control levels reversed the long-term decline in neurogenic capacity. Limiting post-injury neurogenesis reduced early increases in dentate excitability and seizure susceptibility. Our results challenge the assumption that increased neurogenesis after brain injury is beneficial and show that early post-traumatic increases in neurogenesis adversely affect long-term outcomes by exhausting neurogenic potential and enhancing epileptogenesis. Treatments aimed at limiting excessive neurogenesis can potentially restore neuroproliferative capacity and limit epilepsy after brain injury.

INTRODUCTION

Traumatic brain injury (TBI) is a growing epidemic with significant long-term neurocognitive disorders including impaired memory processing and epilepsy (Pitkanen et al., 2014). TBI is characterized by several cellular and circuit changes (Atkins, 2011; Cohen et al., 2007), which shape the long-term neurological sequelae (Herman, 2002). In addition to the well-documented dentate neuronal loss (Gupta et al., 2012; Neuberger et al., 2014), there is an increase in the generation of new neurons in the dentate gyrus within days after TBI (Dash et al., 2001; Kernie and Parent, 2010; Yu et al., 2008). How these newly born neurons modify functional outcomes after brain injury is not fully understood.

The subgranular zone of the adult dentate gyrus has been proposed as a niche region for neural stem cells that supports constitutive neurogenesis throughout postnatal life. However, the rate of neurogenesis can be altered physiologically with aging and in disease such as temporal lobe epilepsy, TBI, ischemia, and stroke (Connor, 2012). Since dentate neurogenesis is proposed to replace lost neurons (Yu et al., 2008), the increase in neurogenesis after TBI may promote recovery (Sun et al., 2007; Yu et al., 2016b). However, a rapid expansion of stem cell populations in certain pathological conditions can deplete stem cells (Jacob and Osato, 2009) due to cell death, fate change, or cellular senescence (Artegiani and Calegari, 2012). Thus an expansion in neurogenesis could paradoxically deplete neural precursor cell populations over time and limit the normal capacity to replace damaged cells and repair the network. Whether the post-injury increase in neurogenesis is sustained or undermines the long-term capacity for neurogenesis remains to be examined.

While prior studies have examined outcomes after ablating both normal and injury-induced neurogenesis (Blaiss et al., 2011), targeting mechanisms that augment neurogenesis after injury is a promising strategy to examine the consequence of excess neurogenesis without eliminating physiological neurogenesis. In the adult dentate, vascular endothelial growth factor A (VEGF-A), acting through VEGF receptor 2 (VEGFR2) localized in neural precursor cells (Kirby et al., 2015; Segi-Nishida et al., 2008), has been shown to increase proliferation, survival, and integration of newborn neurons (Louissaint et al., 2002; Shen et al., 2004). Recent studies have identified increased VEGF-A levels after TBI and demonstrated that blocking VEGFR2 signaling reduces post-injury increases in neurogenesis (Lu et al., 2011; Shore et al., 2004). Thus, VEGFR2 could be targeted to limit enhanced post-traumatic neurogenesis without eliminating physiological neurogenesis.

Apart from effects on neurogenic capacity, whether excessive neurogenesis after TBI may contribute to lasting pathology is an open question. In experimental epilepsy, a population of granule cells born after seizures gives rise to aberrant connections, which could increase network excitability and promote epilepsy (Cha et al., 2004; Parent et al., 1997). Development of epilepsy after a latent period is a major consequence of brain injury, raising the possibility that post-injury increase in neurogenesis may render the hippocampus more excitable and susceptible to seizures. By systematically evaluating

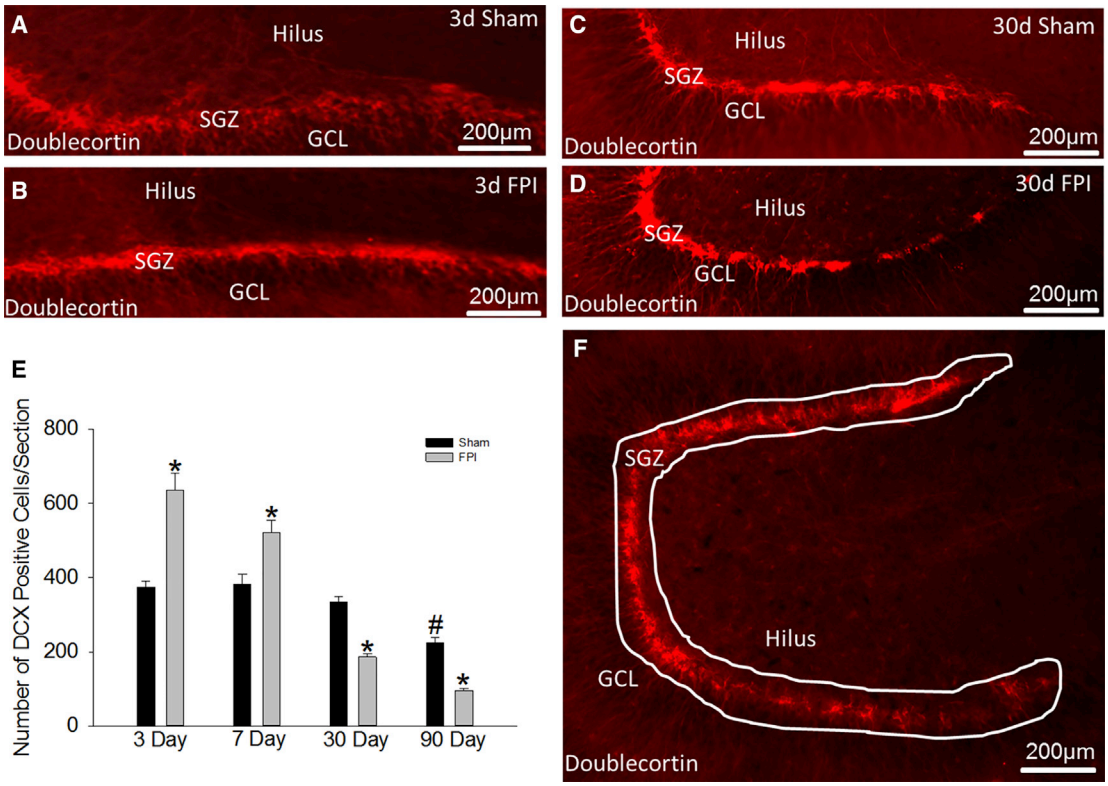

Figure 1. Biphasic Changes in Neurogenesis after Brain Injury

(A–D) Images show doublecortin (DCX) immunostaining in sections from rats sacrificed 3 days (A, sham; B, FPI) and 30 days (C, sham; D, FPI) after moderate FPI or sham injury.

(E) Quantification of DCX-labeled cells in sections from rats sacrificed 3, 7, 30, and 90 days after FPI are compared with data from age-matched sham-injured controls. Main effect of injury on DCX cell counts $F_{(1,\ 26)} = 1.378$; $p = 0.251$. Main effect of post-injury time on DCX cell counts $F_{(3,\ 26)} = 26.576$; $p < 0.001$. Interaction between injury and time was significant ($F_{(3,\ 26)} = 10.514$; $p < 0.001$).*$p < 0.05$ compared with sham and $^{\#}p < 0.05$ compared with 3-day sham by two-way ANOVA (TW-ANOVA) and pairwise post hoc comparisons. n = 4 sham and 5 FPI rats/group. Pairwise comparisons between all FPI groups were significant.

(F) Example of the contour tracing used to outline the dentate subgranular zone for stereological cell counts.

d, day; GLC, granule cell layer; SGZ, subgranular zone. Data are presented as means ± SEM.

neurogenesis, proliferation rates, neuroproliferative capacity, and network excitability after brain injury, we test the prevailing assumption that increased neurogenesis after TBI is beneficial.

RESULTS

Transient Increase in Neurogenesis after TBI is Followed by Long-Term Decline

Immature granule cells (IGCs) expressing doublecortin (DCX) are known to increase within days after brain injury (Kernie and Parent, 2010; Sun et al., 2007). We determined whether this increase is sustained by systematically quantifying DCX-expressing IGCs 3, 7, 30, and 90 days after fluid percussion injury (FPI) and sham injury. Consistent with previous studies, IGCs on the injured side almost doubled 3 days after injury (Figure 1E; DCX cells/section, sham: 370 ± 22; FPI: 638 ± 59; n = 4 rats, $p < 0.05$) while IGCs on the uninjured contralateral side were unchanged (Figure S1A). However, IGC counts were significantly reduced (Figures 1C–1E) 30 days after FPI and were less than half that of age-matched sham controls 90 days after injury (Figure 1E; DCX cells/section, sham: 225 ± 32, n = 4 rats; FPI: 96 ± 2, n = 5 rats; $p < 0.05$). The data demonstrate that despite early increases 3–7 days post FPI, neurogenesis in the injured dentate declines by 30 days. These findings raise the possibility of a progressive loss of IGCs and neural progenitor cells or an exhaustion of NPC proliferative capacity after brain injury.

Altered NPC Proliferation Drives Post-injury Changes in Neurogenesis

We sought to determine whether the biphasic post-traumatic changes in IGC numbers resulted from progressive

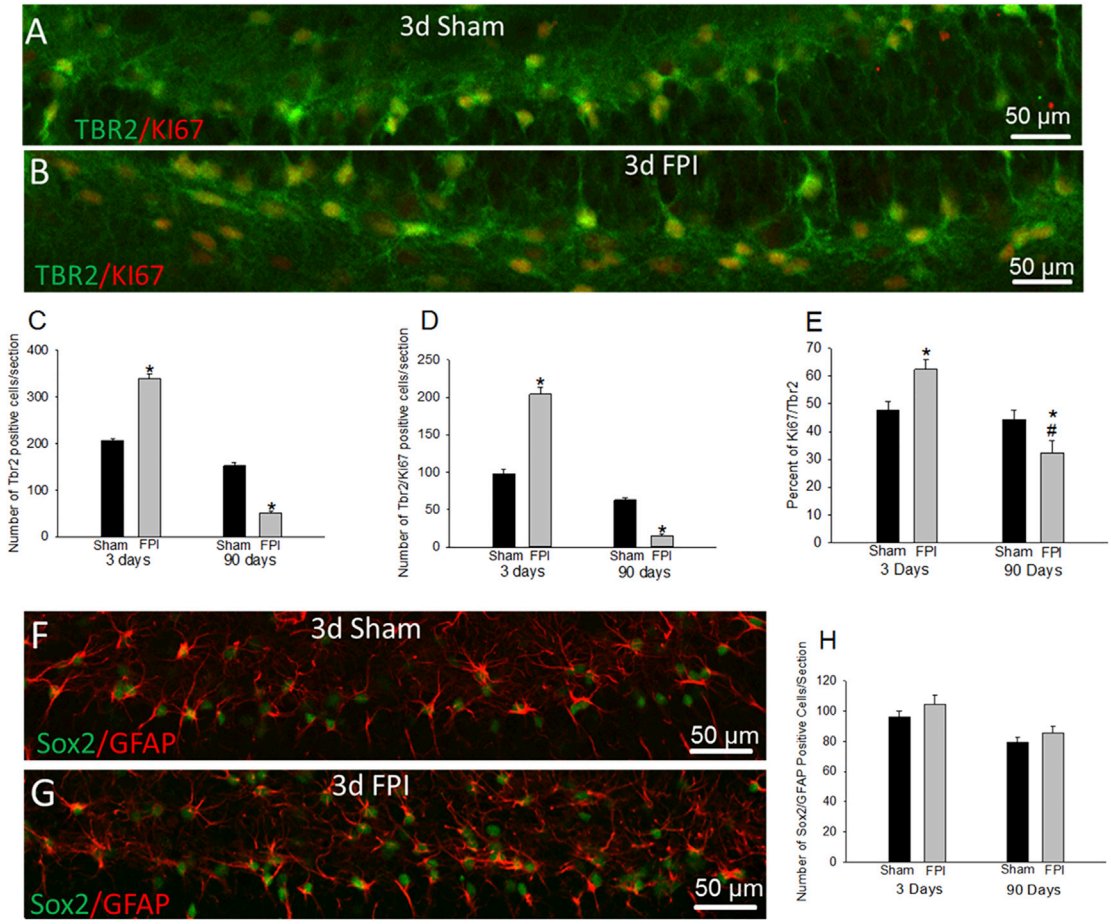

Figure 2. Alterations in NPC Proliferation Rates Drive Post-injury Changes in Neurogenesis

(A and B) Confocal images of sections from rats 3 days after sham (A) or FPI (B) shows NPCs co-labeled for Tbr2 and Ki67.

(C and D) Stereological quantification of TBR2-positive cells (C) and TBR2 and Ki67 co-labeled cells (D) in sections 3 and 90 days after FPI or sham injury.

(E–G) Summary plot (E) of the percentage of proliferating NPCs quantified as the number of Tbr2/Ki67 co-labeled cells normalized to the number of Tbr2 cells in the slice. There was a significant effect of injury and time on both the total number of NPCs (injury: $F_{(1, 14)} = 6.417$; $p = 0.024$; time: $F_{(1, 14)} = 742.891$; $p < 0.001$) and proliferation (injury: $F_{(1, 14)} = 60.263$; $p < 0.001$; time: $F_{(1, 14)} = 902.173$; $p < 0.001$). Interaction between injury and time was also significant for both NPCs ($F_{(1, 14)} = 346.370$; $p < 0.001$) and proliferation ($F_{(1, 14)} = 422.151$; $p < 0.001$), reflecting the early increase and late decline. n = 4 sham and 5 FPI rats/group. Confocal images of sections from rats 3 days after sham (F) or FPI (G) shows type I stem cells co-labeled for Sox2 and GFAP.

(H) Summary plot of Sox2 and GFAP co-labeled cells. Effect of time on the total number of co-labeled cells (time: $F_{(1, 12)} = 14.641$; $p = 0.002$) was significant. However, effect of injury ($F_{(1, 12)} = 2.409$; $p = 0.147$) and interaction between injury and time were not significant ($F_{(1, 12)} = 0.0582$; $p = 0.814$). n = 4 sham and 4 FPI rats/group.

*$p < 0.05$ compared with age-matched sham and $^{\#}p < 0.05$ compared with sham at 3 days for pairwise comparisons following TW-ANOVA. Note the difference in scale of y axis in (C) to (E). Data are presented as means ± SEM.

changes in NPC proliferation or early accumulation of maturation-incompetent IGCs followed by enhanced degeneration. Hippocampal sections from rats 3 and 90 days after FPI and sham injury were labeled for Tbr2 (T-box brain protein 2), a marker for NPCs, and Ki67 expressed in proliferating cells. Both the total number of Tbr2-positive NPCs and Ki67-expressing proliferating cells were increased 3 days after injury (Figures 2A–2D, S2A, and S2B; $Tbr2^+$ cells/section, sham: 206 ± 5, n = 4 rats; FPI: 339 ± 10, n = 5 rats; $p < 0.05$; $Ki67^+$ cells/section, sham: 98 ± 5, n = 4 rats; FPI: 204 ± 4, n = 5 rats; $p < 0.05$). The proportion of NPCs co-labeled for Ki67 increased 3 days after FPI, indicating enhanced NPC proliferation (Figure 2E; % NPCs expressing Ki67, sham: 47.8% ± 2.9%, n = 4 rats; FPI: 62.4% ± 3.6%, n = 5 rats; $p < 0.05$). However, both NPC numbers and proliferating cells were significantly

decreased 90 days post injury (Figures 2C and 2D; $Tbr2^+$ cells/section, sham: 152 ± 5, n = 4 rats; FPI: 52 ± 1, n = 5 rats; $p < 0.05$; $Ki67^+$ cells/section, sham: 63 ± 3, n = 4 rats; FPI: 15 ± 2, n = 5 rats; $p < 0.05$). Crucially, the percentage of proliferating NPCs was significantly reduced 90 days post injury (Figure 2E; %NPCs expressing Ki67, sham: 44.4% ± 3.4%, n = 4 rats; FPI: 32.4% ± 4.4%, n = 5 rats; $p < 0.05$). Examination of type I neural stem cells, co-labeled for Sox-2, a marker for type 1 and type 2 stem cells, and glial fibrillary acidic protein (GFAP), a marker for type I neural stem cells, revealed no differences between groups at 3 or 90 days (Figures 2F–2H; $Sox2/GFAP^+$ cells/section, 3 days: sham: 96 ± 4, FPI: 104 ± 7; $p > 0.05$; 90 days: sham: 79 ± 3, FPI: 85 ± 4, n = 4 rats each; $p > 0.05$). There was, however, significant reduction in type I stem cells between 3 and 90 days, which is consistent with a decline in stem cells with age. Overall, the type I stem cells were unchanged and the proportion of proliferating NPCs increased to 62.4% ± 3.6% 3 days after FPI and declined to 32.4% ± 4.4% at 90 days while proliferation levels in controls was unchanged, suggesting that changes in NPC proliferation rates may underlie the biphasic alterations in neurogenesis after TBI.

Newborn Neurons Generated after TBI Survive and Mature into Granule Cells

We examined whether progressive degenerative loss could contribute to long-term decline in IGC numbers after FPI. Although we have demonstrated dentate neuronal degeneration 4 hrs after FPI (Neuberger et al., 2014), Fluoro-Jade C staining of sections 3, 7, 30, and 90 days after FPI failed to reveal degenerating cells (data not shown, n = 3 rats/group/time point). Similarly, the number of TUNEL-stained apoptotic cells in the subgranular zone did not differ between sham and FPI groups at 3 and 7 days (Figures S3A and S3B). Thus, IGC or NPC degeneration is unlikely to underlie a decline in IGCs after FPI.

To determine the fate of IGCs born early after FPI, we pulse-labeled proliferating NPCs with bromodeoxyuridine (BrdU) 0–4 days after injury and quantified their survival and maturation 45 days post injury (Figure S4A). Sections from rats sacrificed 45 days after FPI showed more BrdU-positive profiles than shams, indicating that IGCs born after injury survive. Co-labeling for BrdU and Prox-1, a marker for mature granule cells, identified a 64% increase in co-labeled cellular profiles after FPI compared with shams, demonstrating that proliferating cells born after injury mature into granule cells (Figures S4B–S4D). While not all hilar BrdU cells expressed Prox-1, all BrdU-labeled cells in the granule cell layer expressed Prox-1 and a majority were located in the inner third of the granule cell layer. Unlike observations in experimental epilepsy (Parent et al., 1997), BrdU-Prox-1 co-labeled cells were not present in ectopic locations including the hilus. These data indicate that the increase in IGCs early after injury results in mature neurons, which survive and integrate into the granule cell layer.

VEGFR2 Antagonist Eliminates Early Increases in Neurogenesis after TBI

The biphasic change in post-traumatic neurogenesis is reminiscent of stem cell exhaustion observed in hematological pathologies (Jacob and Osato, 2009) whereby there is a causal association between increased NPC proliferation and subsequent decline. To assess whether post-traumatic neurogenesis follows a similar trend, we sought to reduce injury-induced increases in neurogenesis without ablating NPCs or suppressing physiological neurogenesis. It has been shown that increases in VEGF-A acting through its receptor VEGFR2, selectively expressed in dentate neural stem and precursor cells (Kirby et al., 2015), regulates neurogenesis after TBI and that VEGFR2 antagonists suppress neurogenesis after TBI (Lu et al., 2011). Therefore, we tested whether the selective VEGFR2 antagonist, SU1498 (5 μg/μL; 2-μL bolus intracerebroventricularly [ICV], 2 hr post injury) (Lu et al., 2011) could reduce FPI-induced neurogenesis to control levels. SU1498- and vehicle-treated rats were sacrificed 3 days after FPI to quantify DCX expression (Figure 3A). SU1498 reduced neurogenesis in both sham (Figure 3B; DCX cells/section, sham: 375 ± 27, n = 4 rats; sham-SU1498: 245 ± 6, n = 4 rats; $p < 0.05$) and FPI rats (Figure 3B; DCX cells/section, FPI: 643 ± 20, n = 4 rats; FPI-SU1498: 399 ± 5, n = 5 rats; $p < 0.05$). IGC counts in vehicle-treated FPI rats were not different from those in untreated FPI rats (Figure 3B; DCX cells/section, FPI-DMSO: 623 ± 19, n = 3 rats; FPI: 643 ± 20, n = 4 rats; $p > 0.05$). Importantly, VEGFR2 antagonist returned FPI-induced neurogenesis at 3 days post injury to levels comparable with untreated sham controls (Figure 3B; DCX cells/section, sham: 375 ± 27, n = 4 rats; FPI-SU1498: 399 ± 5, n = 5 rats; $p > 0.05$). SU1498 also reduced post-FPI neurogenesis compared with both untreated and vehicle-treated FPI (Figure 3B; DCX cells/section, FPI: 643 ± 20, n = 4 rats; FPI-DMSO: 623 ± 19, n = 3 rats; FPI-SU1498: 399 ± 10, n = 5 rats; $p < 0.05$). Immunostaining for Tbr2 and Ki67 revealed that blocking VEGFR2 restores NPC proliferation rates 3 days post injury to levels comparable with untreated shams (Figure 3C; $Tbr2/Ki67^+$ cells/section, sham: 97 ± 5; FPI-SU1498: 107 ± 7; n = 4 rats each; $p > 0.05$). As with injury, SU1498 treatment did not alter neurogenesis in the contralateral dentate (Figure S1A). These data suggest that VEGF-A/VEGFR2 signaling contributes to the early post-injury neurogenic burst. Although prolonged VEGFR2 antagonist infusion was shown to increase dentate neurodegeneration after FPI (Lee and Agoston, 2009), Fluoro-Jade (not shown) and TUNEL labeling of sections 3 days

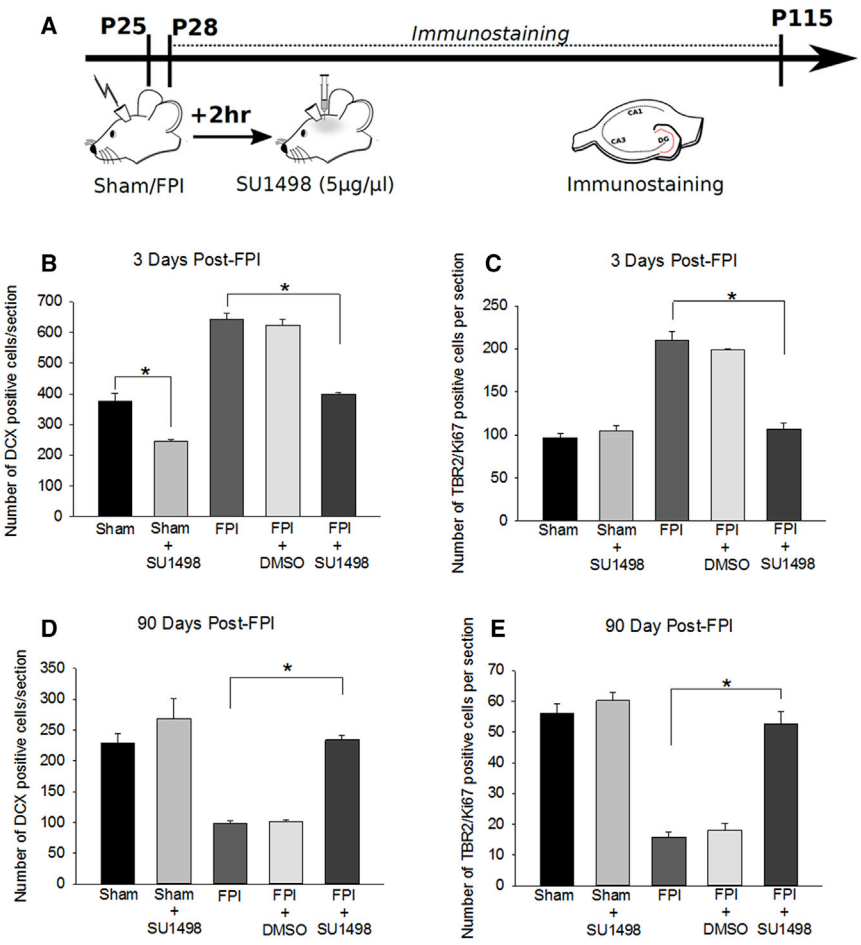

Figure 3. Blocking Early Post-injury Increase in Neurogenesis Prevents Long-Term Decline

(A) Schematic of the experimental timeline. (B and C) Summary of the stereological quantification of DCX-expressing IGCs (B) and Tbr2/Ki67 double-labeled proliferating NPCs (C) in sections obtained 3 days after FPI. (D and E) Summary of the stereological quantification of DCX-expressing IGCs (D) and Tbr2/Ki67 double-labeled proliferating NPCs (E) 90 days after injury. Three days post FPI, effects of injury (IGCs: $F_{(1, 16)} = 185.110$; $p < 0.001$; NPCs: $F_{(1, 13)} = 71.859$; $p < 0.001$) and antagonist treatment (IGCs: $F_{(1, 16)} = 144.326$; $p < 0.001$; $F_{(1, 13)} = 47.886$; $p < 0.001$) were significant. The interaction between injury and antagonist was also significant for both IGCs ($F_{(1, 16)} = 11.953$; $p = 0.003$) and NPCs ($F_{(1, 13)} = 67.350$; $p < 0.001$). Ninety days post FPI, the main effect of injury (IGCs: $F_{(1, 17)} = 32.880$; $p < 0.001$; NPCs: $F_{(1, 13)} = 69.176$; $p < 0.001$), antagonist treatment (IGCs: $F_{(1, 17)} = 37.022$; $p < 0.001$; $F_{(1, 13)} = 50.320$; $p < 0.001$), and interaction between injury and antagonist (IGCs: $F_{(1, 17)} = 11.051$; $p = 0.004$; NPCs: $F_{(1, 13)} = 31.837$; $p < 0.001$) on the total number of IGCs and NPCs was significant.
n = 3–4 sham and 3–5 FPI rats/group. *$p < 0.05$ by pairwise comparison following TW-ANOVA. Note the difference in scale of y axis in (B) to (E). Data are presented as means ± SEM.

after FPI revealed no difference between SU1498- and vehicle-treated rats (n = 4 rats/group, Figure S3A).

Since VEGFR2 is expressed by multiple cell types (Cao et al., 2004; Lee and Agoston, 2009), we tested the potential for non-specific effects of VEGFR2 independent of neurogenesis. However, VEGFR2 treatment did not alter the pattern of dentate hilar neuronal loss examined by Nissl stain (Figures S5A–S5D) or astrogliosis revealed by GFAP labeling (Figures S5E and S5F) in sections 3 days after FPI. For our purpose, these data demonstrate that VEGFR2 antagonism reduces early post-FPI neurogenesis to control levels without increasing neurodegeneration or modifying early hilar neuronal loss or astrogliosis, and validates the use of SU1498 to test the causal association between the post-FPI increase in neurogenesis and the ensuing decline.

Suppressing Post-injury Excess Neurogenesis Prevents Long-Term Decline in Neurogenesis

Next, a cohort of SU1498- and vehicle-treated rats were sacrificed after 90 days and examined for DCX immunostaining (Figure 3A). As predicted, SU1498 treatment restored IGCs in rats 90 days after FPI to levels comparable with age-matched controls (Figure 3D; DCX cells/section, sham: 229 ± 15, n = 4 rats; sham-SU1498: 269 ± 32, n = 4 rats; FPI-SU1498: 234 ± 8, n = 5 rats; $p > 0.05$). The number of IGCs in SU1498-treated rats 90 days after FPI was significantly higher than in age-matched untreated FPI rats (Figure 3D; DCX cells/section, FPI: 99 ± 4, n = 5 rats; FPI-SU1498: 234 ± 8, n = 5 rats; $p < 0.05$). IGCs in vehicle-treated and untreated FPI rats were not different at 90 days (Figure 3D; DCX cells/section, FPI: 99 ± 4, n = 5 rats; FPI-DMSO: 102 ± 3, n = 3 rats; $p > 0.05$ by t test). In sections obtained 90 days post injury, labeling for Tbr2 and Ki67 demonstrated that SU1498 treatment restored the number of proliferating NPCs to control levels (Figure 3E; TBR2/Ki67$^+$ cells/section, sham: 56 ± 5, n = 3 rats; FPI: 16 ± 2, n = 4 rats; FPI-SU1498: 53 ± 4, n = 4 rats; $p > 0.05$). In contrast, co-labeling for Sox2 and GFAP revealed no significant effect of SU1498 on type I stem cells 3 or 90 days post TBI (Figures S1B and S1C). These data imply that the long-term decrease in IGCs observed 30 and 90 days after FPI is a consequence of the early post-injury

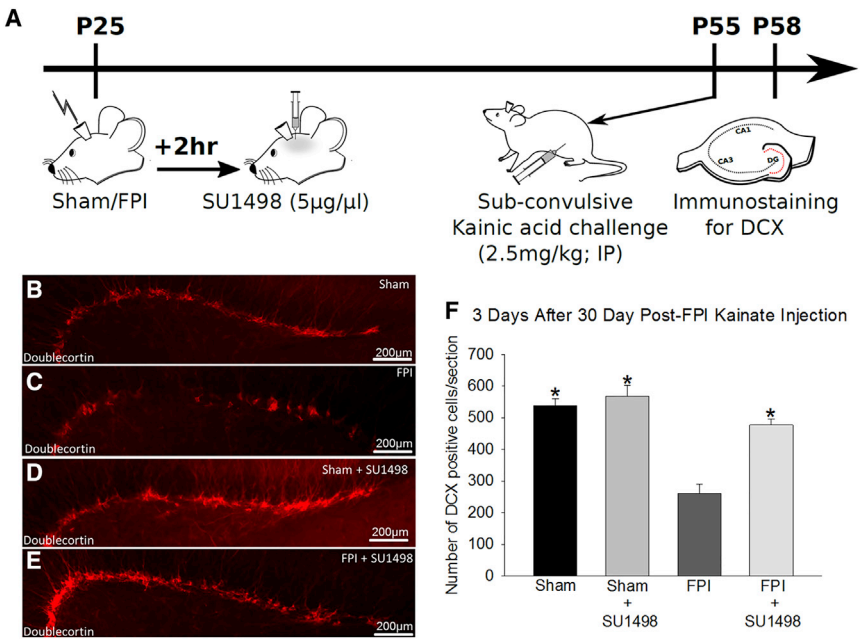

Figure 4. VEGFR2 Antagonist Treatment Improves Long-Term Deficits in Neurogenic Potential after FPI

(A) Schematic of experimental timeline.

(B–E) Images show doublecortin (DCX) immunostaining in sections from rats sacrificed 3 days after subconvulsive kainic acid challenge (B, sham; C, FPI; D, sham + SU1498; E, FPI + SU1498) following FPI or sham injury.

(F) Stereological quantification of DCX-positive IGCs in sections from rats 3 days after kainic acid challenge. There was a significant effect of injury ($F_{(1, 17)} = 12.523$; $p = 0.003$), antagonist treatment ($F_{(1, 17)} = 27.370$; $p < 0.001$), and interaction between injury and antagonist ($F_{(1, 17)} = 14.760$; $p = 0.001$) on long-term neurogenic capacity. n = 3 sham and 4 FPI rats/group.

*p < 0.05 compared with age-matched sham by pairwise comparisons following TW-ANOVA. Data are presented as means ± SEM.

neurogenic burst and the resulting exhaustion of NPC proliferative capacity.

Post-traumatic Decline in Neurogenic Potential is Rescued by Limiting Early Increases in Neurogenesis

To directly evaluate the effect of injury-induced neurogenesis on NPC proliferative capacity, we challenged vehicle and SU1498-treated FPI and sham rats with a subconvulsive dose of kainic acid (KA) (2.5 mg/kg, intraperitoneally [i.p.]) 30 days after FPI when neurogenesis is reduced. At this dose KA increases neurogenesis, providing a measure of NPC proliferative capacity (Sierra et al., 2015). Rats were observed for 3 hr after injection to rule out behavioral seizures and sacrificed 3 days after KA challenge to quantify DCX-positive IGCs (Figure 4A). KA challenge increased neurogenesis in untreated, vehicle-treated, and SU1498-treated controls (Figures 4A–4F; DCX cells/section, sham: 565 ± 31, n = 3 rats; sham-DMSO: 514 ± 26, n = 3 rats; sham-SU1498: 568 ± 34, n = 4 rats after KA versus sham and 336 ± 22, n = 4 rats without KA). Data from untreated and vehicle-treated shams were not statistically different and were combined for further analysis. As predicted, brain-injured rats challenged with KA had fewer IGCs than shams that received the same treatments (Figure 4F; DCX cells/section, sham: 565 ± 31, n = 3 rats; FPI: 261 ± 30, n = 4 rats; $p < 0.05$), demonstrating that FPI reduces the long-term neurogenic response. Importantly, SU1498 treatment augmented the number of IGCs generated in injured rats in response to the KA challenge (Figure 4F; DCX cells/section, FPI: 261 ± 30, n = 4 rats; FPI-SU1498: 477 ± 19, n = 4 rats; $p < 0.05$), restoring neurogenic capacity to control levels. Together, these data demonstrate that the early increase in neurogenesis after TBI results in exhaustion of the neuroproliferative capacity and underlies long-term deficits in neurogenesis.

Limiting Early Post-injury Neurogenesis Reduces Dentate Excitability and Seizure Susceptibility

Experimental FPI is known to enhance dentate network excitability at 1 week and contribute to long-term increase in seizure susceptibility and temporal lobe epilepsy (Gupta et al., 2012; Kharatishvili et al., 2006). While VEGFR2 antagonist reduces early post-injury increases in neurogenesis, VEGFR2 signaling has been shown to acutely reduce neuronal excitability (McCloskey et al., 2005; Sun and Ma, 2013), raising the possibility that our treatment may augment network excitability. To examine the effects of the brief SU1498 treatment on excitability, we sacrificed vehicle and SU1498-treated rats 1 week after FPI or sham injury and examined perforant path-evoked granule cell field responses *ex vivo* (Figure 5A). Consistent with earlier studies (Neuberger et al., 2014), afferent-evoked granule cell population spike amplitude was enhanced in vehicle-treated FPI rats (Figures 5B and 5C; amplitude at 0.5 mV stimulation, in mV: sham-DMSO: 0.30 ± 0.07, n = 5 rats; FPI-DMSO: 0.73 ± 0.15, n = 5 rats; $p < 0.05$). Curiously, population spike amplitude in SU1498-treated FPI rats was decreased compared with vehicle-treated FPI rats (Figures 5B and 5C; amplitude at 0.5 mV stimulation, in mV: FPI-DMSO: 0.73 ± 0.15, n = 5 rats; FPI-SU1498: 0.27 ± 0.06, n = 5 rats; $p < 0.05$) and were not different from sham controls. Thus, the bolus VEGFR2 antagonist treatment used

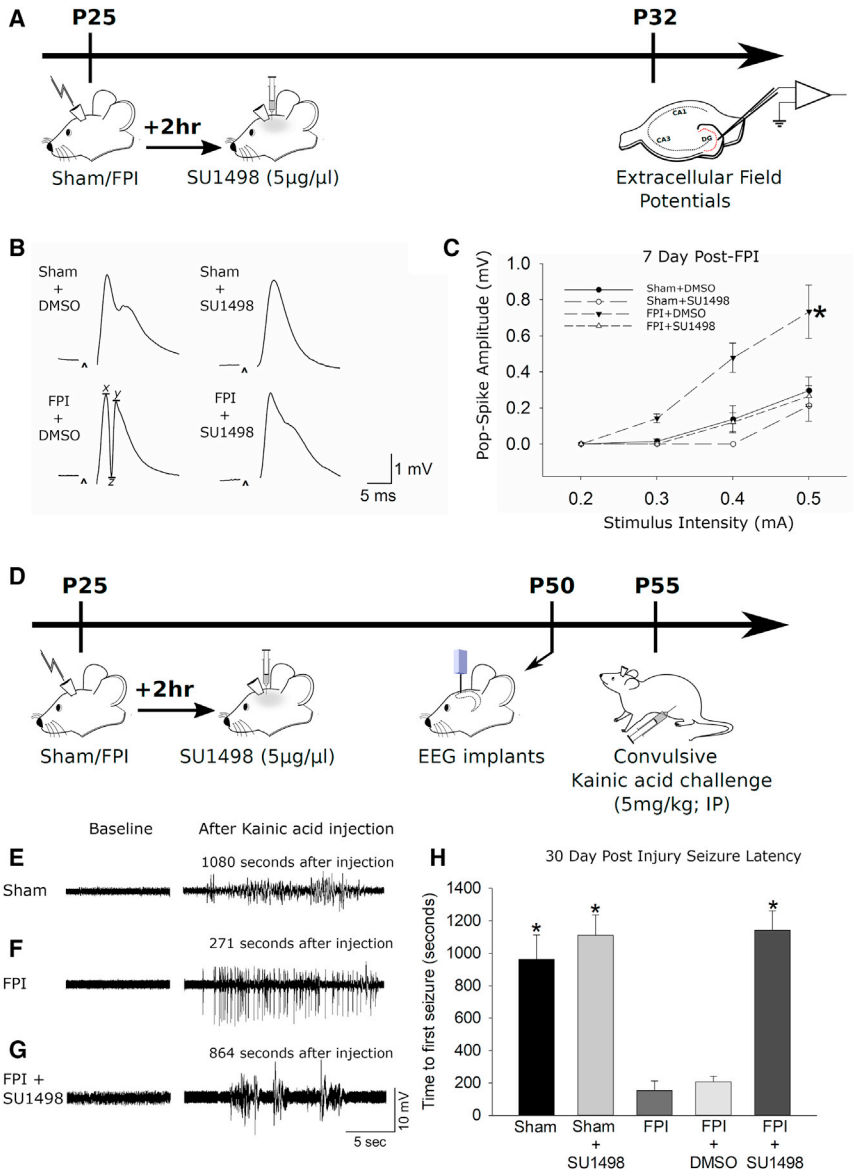

Figure 5. VEGFR2 Antagonist Reduces Excitability 1 Week after TBI and Reduces Seizure Susceptibility after TBI

(A) Schematic of experimental timeline.

(B) Examples of voltage traces of dentate granule cell field responses evoked by a 0.5-mA stimulus to the perforant path. Recordings were performed in control artificial cerebrospinal fluid (aCSF). Population spike amplitude was calculated as $(x + y)/2 - z$.

(C) Summary plot of afferent evoked population spike amplitude in aCSF. There was a significant effect of both injury ($F_{(1,\ 16)}$ = 6.400; p = 0.022) and antagonist treatment ($F_{(1,\ 16)}$ = 7.900; p = 0.013) on excitability. The interaction between injury and antagonist was $F_{(1,\ 16)}$ = 3.014; p = 0.102. n = 5 sham and 5 FPI rats/group. *p < 0.05 by mixed-design ANOVA.

(D) Schematic of the timeline for FPI/sham injury followed by drug infusion, EEG electrode implantation and subsequent video-EEG monitoring during kainic acid challenge.

(E–H) Representative baseline (left) and convulsive (right) EEG traces recorded in rats 30 days after FPI (E, sham; F, FPI; G, FPI + SU1498). Time of recording is indicated above each trace. (H) Summary plot of time in seconds to first seizure following a convulsive dose of kainate injection. There were significant main effects of injury ($F_{(1,\ 17)}$ = 12.523; p = 0.003) and antagonist treatment ($F_{(1,\ 17)}$ = 27.370; p < 0.001) on seizure latency. The interaction between injury and antagonist was also significant ($F_{(1,\ 17)}$ = 14.760; p = 0.001). n = 4–5 sham and 3–5 FPI rats/group.

*p < 0.05 by pairwise comparisons with FPI and FPI-vehicle following TW-ANOVA. Data are presented as means ± SEM.

here does not enhance network excitability. Rather, it is possible that the reduction in dentate excitability is a consequence of previously unrecognized contribution of enhanced neurogenesis to early post-traumatic dentate hyperexcitability.

Brain injury can increase seizure susceptibility by a convergence of mechanisms that are not fully understood (Hunt et al., 2013). While increases in network excitability could augment seizure susceptibility, enhanced neurogenesis in experimental epilepsy has been implicated in the formation of abnormal circuits that promote the development of epilepsy (Danzer, 2008). However, whether neurogenesis contributes to enhanced seizure susceptibility after TBI has not been examined. Previous studies have shown that FPI leads to spontaneous seizures after a prolonged latent period (Kharatishvili et al., 2006) and have used latency to chemically evoked seizures to assess risk for epilepsy (Echegoyen et al., 2009). We performed video-EEG (electroencephalographic) recordings in rats 1 month after FPI or sham injury to determine the latency to develop seizures following a convulsive dose of KA (5 mg/kg, i.p.). Injured rats developed electrical seizures significantly earlier than shams (Figures 5D–5H; latency in seconds, sham: 963.4 ± 150.1, n = 5; FPI: 153.8 ± 58.3, n = 4; p < 0.05), consistent with enhanced seizure susceptibility after FPI (Echegoyen et al., 2009). Vehicle treatment failed to alter seizure latency (Figures 5E–5H; latency in seconds, FPI: 153.8 ± 58.3, n = 4; FPI-DMSO: 207.7 ± 33.9, n = 3; p > 0.05 by

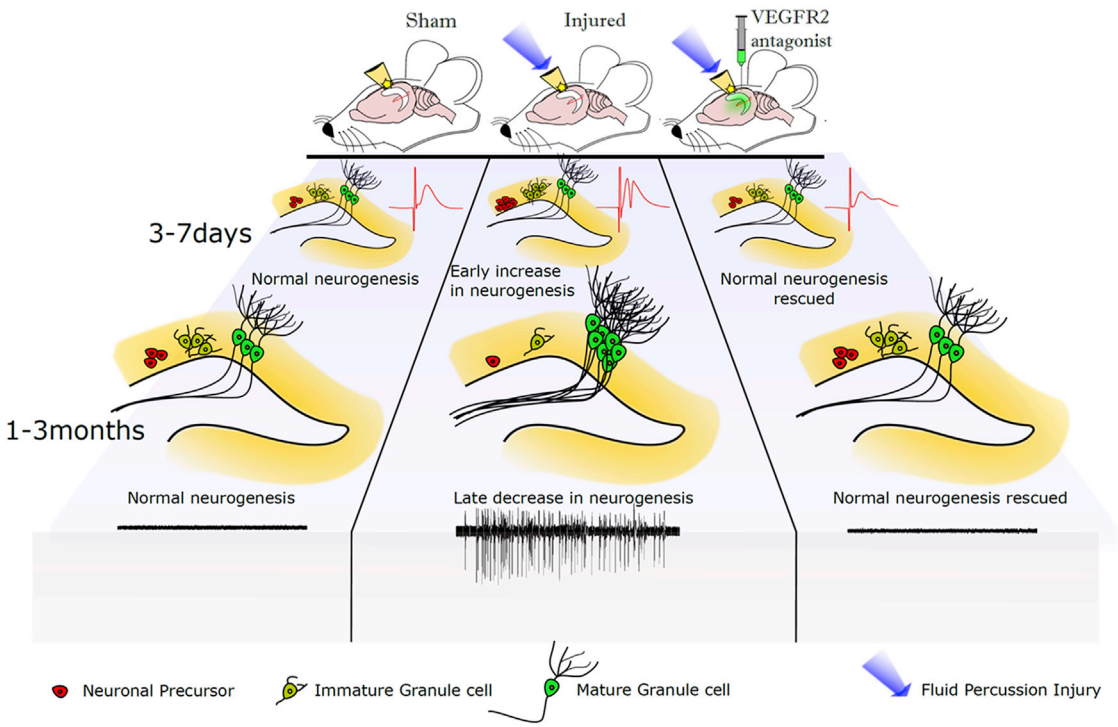

Figure 6. Summary of the Impact of FPI on Neurogenesis and Excitability

Graphical representation of the early (3–7 days) and long-term (30–90 days) changes in neuronal precursors, immature and mature granule cells, and network excitability in sham controls, post-FPI-treated, and post-SU1498-treated FPI rats. Note the increase in neural precursors and IGCs early after injury accompanied by increases in dentate field excitability (red trace) compared with control. Neural precursor and IGC numbers show a later decline accompanied by an increase in mature granule cells derived from maturation of the IGCs born during the early neurogenic burst and seizure susceptibility. VEGFR2 antagonist treatment after FPI reverses the post-injury changes in early NPC proliferation and reverses early and long-term changes in neurogenesis and excitability after brain injury. n = 3–5 animals for all experiments performed. Original artwork and schematic design was by Deepak Subramanian.

t test). Although SU1498 did not alter seizure latency in shams (Figures 5E–5H; latency in seconds, sham: 963.4 ± 150.1, n = 5; sham-SU1498: 1,111.5 ± 125.5, n = 4; $p > 0.05$), it significantly prolonged seizure latency after FPI (Figures 5E–5H; latency in seconds, FPI: 153.8 ± 58.3, n = 4; FPI-SU1498: 1,143.8 ± 118.6, n = 5; $p < 0.05$). These data demonstrate that blocking the initial increase in neurogenesis improves functional outcomes by reducing susceptibility to chemically evoked seizures.

DISCUSSION

Adult neurogenesis is considered beneficial, replacing lost neurons, enhancing plasticity, and supporting memory formation (Sun, 2014). However, whether augmenting neurogenesis is equally beneficial under pathological conditions is unresolved (Yu et al., 2016b). This study examined the cellular processes underlying the neurogenic burst after brain injury and its effect on long-term outcomes. We demonstrate that the post-injury increase in dentate neurogenesis is transient and gives way to a marked reduction by 30 days. As summarized in Figure 6, we identify that brain injury transiently enhances NPC proliferation and augments the generation of newborn neurons, which survive and mature into granule cells. We find that the neurogenic burst depletes proliferating NPCs, precipitating a long-term decline in both basal and stimulus-evoked neurogenesis. Suppressing the post-injury neurogenic burst to control levels reduced the early increase in dentate excitability after brain injury and reversed the long-term increase in susceptibility to chemically evoked seizures. These findings indicate that granule cells born early after injury contribute to abnormal network excitability and could support epileptogenesis after brain injury. Together our data demonstrate that excess post-injury neurogenesis contributes to subsequent decline in neuroproliferation and enhanced risk for seizures, and suggest that blocking rather than enhancing neurogenesis will improve long-term neurological outcome.

Although the post-traumatic burst in DCX-expressing IGCs is well documented (Kernie and Parent, 2010), we

demonstrate that the increase in IGCs results from an increase in the number of actively dividing NPCs. IGCs born after injury mature into granule cells (Villasana et al., 2015) (Figure S4), eliminating the possibility that maturation-incompetent IGCs underlie the observed increase. The post-injury IGC burst is early and transient: IGCs almost double 3 days after injury and are progressively reduced by 30 days. The long-term decrease in DCX-positive neurons after brain injury is consistent with an earlier report (Atkins et al., 2010) and is associated with reduced NPC proliferation and a diminished capacity to enhance neurogenesis in response to excitotoxic challenge. Notably, both reduction in NPC proliferation and neurogenic response were restored when the post-traumatic NPC proliferative burst was reduced to control levels, revealing a causal link between the early increase in NPC proliferation and the delayed decrease in neurogenesis. Thus, brain injury results in exhaustion of the "stem cells" of the subgranular neuroproliferative zone in a manner similar to aging (Encinas et al., 2011) or leukemia (Jacob and Osato, 2009). Our findings demonstrating exhaustion of neuroproliferative capacity inform current controversies regarding the true "stem cell" capacity of the hippocampal neurogenic niche (Walker et al., 2008) and support the proposal that dentate neurogenesis is maintained by precursor cells with finite proliferative capacity (Bull and Bartlett, 2005; Encinas et al., 2011). Consequently, brain injury may precipitate an "accelerated aging" with depletion of NPCs, resulting in near exhaustion of the proliferative capacity and long-term cognitive deficits after TBI (Whiting et al., 2006).

Our study used SU1498, a VEGFR2 antagonist previously reported to provide selective mechanistic suppression of post-injury increase in IGCs (Lu et al., 2011). In the adult subgranular zone, VEGFR2 is expressed exclusively in neural stem and precursor cells where it regulates proliferation (Kirby et al., 2015). Brain injury rapidly increases hippocampal expression of VEGFR2 and its ligand VEGF-A (Lu et al., 2011; Marti et al., 2000) with VEGF-A increasing within 12 hr and returning to basal levels by 14 days (Lu et al., 2011). Consistent with the role for VEGF2 in increasing NPC proliferation after injury (Lu et al., 2011), the temporal changes in VEGF signaling correlate with the early increase in neurogenesis at 3–7 days followed by decline by 30 days (Figure 1), and SU1498 eliminated the post-traumatic increase in IGCs without affecting hilar cell loss or astrogliosis. The ability of both VEGFR2 antisense oligodeoxynucleotide and SU1498 to similarly reduce the post-traumatic neurogenic burst in earlier studies (Lu et al., 2011) indicates that SU1498 on neurogenesis are specific to VEGFR2 antagonism. Interestingly, at levels used in our study, SU1498 reduced post-traumatic NPC proliferation without altering proliferation rates of Tbr2/Ki67-expressing NPCs in controls (Figure 3C), implying a minimal role for VEGFR2 signaling in baseline NPC proliferation. Yet SU1498 reduced DCX-positive IGC numbers in controls (Figure 3B). The paradoxical reduction in IGCs following SU1498 treatment in controls despite the lack of drug effect on NPC proliferation suggests a possible role for VEGFR2 signaling in altering the time course of IGC maturation. The selective VEGFR2-dependent regulation of NPC proliferation after TBI provided a powerful experimental opportunity to suppress excess NPC proliferation without perturbing basal proliferation as occurs with irradiation or anti-mitotic agents (Sun et al., 2015; Winocur et al., 2006). Recently, a study demonstrated that precise ablation of actively dividing neural precursors prior to experimental seizures reduced the development of spontaneous seizures (Cho et al., 2015). Our work complements the study by Cho et al. (2015) by using a non-terminal suppression rather than ablation of actively dividing cells, enabling us to assess the role of excess neurogenesis in subsequent loss of neurogenic potential. We show that VEGFR2 suppression after TBI reduces seizure susceptibility without adversely affecting basal neuroproliferation. In contrast to reports that prolonged VEGFR2 antagonist infusion promotes neurodegeneration after TBI (Lee and Agoston, 2009), we observed no evidence for ongoing neurodegeneration following the treatment paradigm used in our study. Furthermore, SU1498 treatment *in vivo* failed to enhance dentate excitability in controls, indicating that VEGF-A-mediated suppression of neuronal excitability, identified in earlier studies (McCloskey et al., 2005; Sun and Ma, 2013), is not compromised by the treatment. Thus, mechanistic suppression of injury-induced neurogenic burst with SU1498 offers the ability to examine the consequences of increased neurogenesis without impairing basal NPC proliferation rates.

Our finding that the post-injury neurogenic burst gives rise to mature granule cells is consistent with published reports (Villasana et al., 2015). This raises the question of how the cohort of "excess" neurons affects network function and long-term outcomes. In murine cortical impact injury, granule cells born after trauma show normal intrinsic physiology (Villasana et al., 2015). An attractive proposal argues that enhanced neurogenesis replaces degenerating neurons after TBI and stabilizes the network (Sun, 2014). In contrast, our findings that suppressing the post-injury neurogenic burst prevents both early increases in dentate network excitability and susceptibility to seizure suggest that the cohort of granule cells developed after injury may form abnormal networks and contribute to long-term pathology. This is not surprising, as brain injury leads to loss of hilar inhibitory and excitatory neurons and not granule cells (Santhakumar et al., 2000; Toth et al., 1997). Since newborn neurons are excitatory, develop

into granule cells, and do not migrate ectopically to the hilus, they are unlikely to compensate for the loss of hilar inhibitory regulation after TBI. Instead, they add excitatory neurons to the network and could contribute to the early post-injury increase in dentate excitability (Gupta et al., 2012; Neuberger et al., 2014). Additionally, these neurons develop in an altered network with reduced hilar inhibitory neurons and mossy cells that innervate and regulate functional maturation of newborn neurons (Chancey et al., 2014). Thus the neurogenic burst after brain trauma is fundamentally different from "physiologically" enhanced states of neurogenesis in exercise and learning, which can enhance cognitive outcomes without promoting pathology.

The ability of the VEGFR2 antagonist treatment to reduce long-term seizure susceptibility is consistent with aberrant network connectivity or function of the cohort of neurons born after injury. However, the ability of the treatment to suppress early dentate excitability 7–9 days after injury is surprising as under physiological conditions, proliferating cells take more than a week to integrate into the network (Kempermann et al., 2015). VEGF-A/VEGFR2 signaling is known to suppress and not to enhance excitability, yet we find that VEGFR2 antagonist reduced excitability in the dentate. Therefore, direct SU1498 modulation of cellular excitability cannot account for the ability of the treatment to reduce dentate excitability after FPI. Since SU1498 has been shown to increase neuronal excitability and did not alter excitability in controls, it is unlikely that the ability of SU1498 to reduce excitability after brain injury results from non-specific effects. The most parsimonious explanation is that the post-injury neurogenic burst contributes to enhanced dentate excitability, suggesting the possibility of accelerated IGC maturation after brain injury. Thus, treatments suppressing excess neurogenic burst may reduce the risk for post-traumatic epileptogenesis by limiting early increases in network excitability and by reducing a cohort of neurons that contribute to lasting changes to the network. It should, however, be noted that post-traumatic epileptogenesis is a complex process involving multiple pathways (Guo et al., 2013; Herman, 2002; Hunt et al., 2013; Pitkanen et al., 2014), and targeting neurogenesis is only one of the strategies used to limit epilepsy after brain injury.

At concentrations used in our study, a single focal injection of SU1498 2 hrs after injury can eliminate excess neurogenesis and restore IGCs to control levels. However, it is possible that limited increases in neurogenesis after TBI may aid in early recovery of circuit function. Previous studies have reported that neurogenesis after TBI aids in improved cognitive performance due to integration of newborn neurons into the dentate circuit (Sun et al., 2007; Yu et al., 2016b). Future work should investigate whether suppression, rather than ablation, of post-injury neurogenic burst affects the recovery of early and long-term memory function and if the post-traumatic loss of neurogenic capacity, identified here, accelerates long-term neurocognitive decline. In addition, the duration after injury during which suppressing NPC proliferation improves outcomes needs to be examined. While we adopted SU1498 ICV injection to ensure localized drug action in the brain, non-invasive brief systemic treatments with SU5416, a novel small-molecule inhibitor of VEGFR-2, or ramucirumab, an anti-VEGFR2 antibody under clinical trial for cancer therapy (Rosen, 2001), could be an option for translation to a clinical setting. Thus it is attractive to propose that the neurogenic potential can be therapeutically harnessed to support long-term memory performance and limit epileptogenesis.

In conclusion, we find that the massive increase in NPC proliferation after brain injury may be doubly detrimental by depleting NPCs and their proliferative capacity reminiscent of accelerated aging and by supporting enhanced excitability and epileptogenesis. Targeted suppression of the early post-injury increase in neurogenesis may improve long-term outcomes after brain injury.

EXPERIMENTAL PROCEDURES

All procedures were approved by the Institutional Animal Care and Use Committee of the Rutgers New Jersey Medical School (Newark, NJ) and are in compliance with the ARRIVE guidelines. Datasets are available from the corresponding author on reasonable request.

Fluid Percussion Injury

Juvenile male Wistar rats (23–25 days old) were subject to moderate (2.0–2.2 atm) lateral FPI or sham injury using established methods (Gupta et al., 2012).

Animals from the same litter were randomly assigned to control or FPI groups. Similarly, FPI and sham rats were randomly assigned to drug or saline groups. FPI rats were excluded from further studies if the injury peak pressure was below 2.0 atm, if the waveform lacked a smooth rise, or if the injured rats showed <10 s apnea.

In Vivo Treatments

Two hours after FPI or sham injury, randomly selected rats underwent stereotaxic injection (26-gauge needles, Hamilton) of either VEGFR2 antagonist, SU1498 (2 μL of a 5 μg/μL solution in 20% DMSO; Calbiochem) or 20% DMSO (vehicle) into the lateral ventricle (anteroposterior [AP]: −1.8; lateromedial [LM]: +2.5; dorsoventral [DV]: −3.5) on the injured side under ketamine (80 mg/kg)-xylazine (10 mg/kg) anesthesia (i.p.). Thirty days after FPI, a subset of vehicle or SU1498-treated rats were challenged with a subconvulsive dose of KA (2.5 mg/kg, i.p., Tocris) and perfused 3 days later.

Histology and Immunohistochemistry

Immunostaining was performed on free-floating sections (40 μm) of FPI and age-matched sham rats perfused with 4% paraformaldehyde 3–90 days after injury. Sections were washed and blocked in 10% normal donkey serum with 0.3% Triton X-100 for 1 hr. For DCX staining, sections were incubated overnight in anti-doublecortin primary antibody (1:100, goat polyclonal; Santa Cruz Biotechnology) in 0.3% Triton X-100 and 2% normal donkey serum. Double staining for Tbr2 and Ki67 was performed by sequential labeling with anti-Tbr2 (1:200, rabbit polyclonal, Millipore) for 1 hr followed by addition of anti-Ki67 (1:150, rat monoclonal, eBioscience) and overnight incubation. Sections were then labeled with fluorescent secondary antibodies: donkey anti-goat Alexa 594 (1:500; Thermo Scientific) to reveal DCX, donkey anti-rabbit Alexa 488 (1:500; Abcam) to reveal Tbr2, and donkey anti-rat Alexa 594 (1:500; Thermo Scientific) to reveal Ki67, and mounted using Vectashield (Vector Laboratories). Controls omitting primary antibody were routinely included.

Quantification was performed using randomized systematic sampling protocols, selecting every 10th section along the septo-temporal axis. Cell counts were performed with the Optical Fractionator probe of Stereo Investigator V.10.02 (MBF Bioscience) at ×100 (oil objective) on an Olympus Bx51 microscope. In each section, the subgranular zone was outlined by a contour traced under an ×10 objective (Figure 1F) and the number of labeled cells was estimated based on planimetric volume calculations (Li et al., 2014).

Field and *In Vivo* Electrophysiology

VEGFR-2 antagonist or vehicle-treated FPI and sham-injured rats were sacrificed 7–9 days after injury for preparation of acute hippocampal slices (400 μm) for examination of perforant path-evoked dentate population responses (Neuberger et al., 2014) by an investigator blinded to treatments. Twenty-five days after injury, a second group underwent stereotaxic surgical implantation of hippocampal depth electrodes (twisted-wire electrode; Plastics One) on the injured side (AP: −3.0; LM: +3.5; DV: −3.7) under surgical isoflurane anesthesia. Rats were allowed to recover for 5–6 days and connected to a custom tethered EEG system (Pinnacle Technologies) interfaced with video monitoring (Yu et al., 2016a). Following 10 min of baseline EEG recordings, rats received a single convulsive dose of KA (5 mg/kg, i.p.) and were continuously monitored by video-EEG for 3 hrs. Electrographic seizures were defined as: (1) repetitive spike- and sharp-wave discharges with a frequency of >1 Hz; (2) amplitude of activity more than 2-fold over baseline activity; and (3) duration >3 s. The EEG signal was processed as described previously (Yu et al., 2016a) and analyzed by an investigator blinded to treatments.

Statistical Analysis

Data were analyzed using two-tailed Student's t test, mixed-design ANOVA, and two-way ANOVA (TW-ANOVA) followed by pairwise multiple comparison by Holm-Sidak method or mixed-design ANOVA as appropriate, using SigmaPlot 12.3 or SPSS. Significance was set to $p < 0.05$. Sample size for histology is number of animals. Sample size was determined prior to experiments to achieve a power of 0.80 and a probability of type I error (α) of 0.05 (Sigma Plot 12.3). Test for normality and equal variance was routinely performed and appropriate statistical tests determined based on outcomes. Unless stated otherwise, averages of counts from 6 to 8 serial sections were used as an individual data point for each animal. Data are shown as mean ± SEM.

SUPPLEMENTAL INFORMATION

Supplemental Information includes Supplemental Experimental Procedures and five figures and can be found with this article online at http://dx.doi.org/10.1016/j.stemcr.2017.07.015.

AUTHOR CONTRIBUTIONS

E.J.N., B.S., L.C., and A.P. performed experiments; E.J.N., B.S., and L.C. analyzed data; E.J.N. and V.S. interpreted results of experiments; E.J.N. prepared figures; E.J.N. and V.S. authored the manuscript; E.J.N., B.S., L.C., and A.P. edited and approved the manuscript. E.J.N. and V.S. were responsible for conception and design of research.

ACKNOWLEDGMENTS

We thank Jenieve Guevarra, Dipika Sekhar, and Ying Li for their helpful comments and technical assistance and Dr. Steve Levison for helpful discussions. We extend a special thanks to Dr. Deepak Subramanian for original artwork and design of schematics and graphical representations. The project was supported by NIH R01NS097750 and R01NS069861, and NJCBIR CBIR16IRG017 and CBIR11PJT003 to V.S.

Received: March 17, 2017
Revised: July 19, 2017
Accepted: July 20, 2017
Published: August 17, 2017

REFERENCES

Artegiani, B., and Calegari, F. (2012). Age-related cognitive decline: can neural stem cells help us? Aging (Albany NY) *4*, 176–186.

Atkins, C.M. (2011). Decoding hippocampal signaling deficits after traumatic brain injury. Transl. Stroke Res. *2*, 546–555.

Atkins, C.M., Truettner, J.S., Lotocki, G., Sanchez-Molano, J., Kang, Y., Alonso, O.F., Sick, T.J., Dietrich, W.D., and Bramlett, H.M. (2010). Post-traumatic seizure susceptibility is attenuated by hypothermia therapy. Eur. J. Neurosci. *32*, 1912–1920.

Blaiss, C.A., Yu, T.S., Zhang, G., Chen, J., Dimchev, G., Parada, L.F., Powell, C.M., and Kernie, S.G. (2011). Temporally specified genetic ablation of neurogenesis impairs cognitive recovery after traumatic brain injury. J. Neurosci. *31*, 4906–4916.

Bull, N.D., and Bartlett, P.F. (2005). The adult mouse hippocampal progenitor is neurogenic but not a stem cell. J. Neurosci. *25*, 10815–10821.

Cao, L., Jiao, X., Zuzga, D.S., Liu, Y., Fong, D.M., Young, D., and During, M.J. (2004). VEGF links hippocampal activity with neurogenesis, learning and memory. Nat. Genet. *36*, 827–835.

Cha, B.H., Akman, C., Silveira, D.C., Liu, X., and Holmes, G.L. (2004). Spontaneous recurrent seizure following status epilepticus enhances dentate gyrus neurogenesis. Brain Dev. *26*, 394–397.

Chancey, J.H., Poulsen, D.J., Wadiche, J.I., and Overstreet-Wadiche, L. (2014). Hilar mossy cells provide the first glutamatergic synapses to adult-born dentate granule cells. J. Neurosci. *34*, 2349–2354.

Cho, K.O., Lybrand, Z.R., Ito, N., Brulet, R., Tafacory, F., Zhang, L., Good, L., Ure, K., Kernie, S.G., Birnbaum, S.G., et al. (2015). Aberrant hippocampal neurogenesis contributes to epilepsy and associated cognitive decline. Nat. Commun. *6*, 6606.

Cohen, A.S., Pfister, B.J., Schwarzbach, E., Grady, M.S., Goforth, P.B., and Satin, L.S. (2007). Injury-induced alterations in CNS electrophysiology. Prog. Brain Res. *161*, 143–169.

Connor, B. (2012). Compensatory Neurogenesis in the Injured Adult Brain (InTech).

Danzer, S.C. (2008). Postnatal and adult neurogenesis in the development of human disease. Neuroscientist *14*, 446–458.

Dash, P.K., Mach, S.A., and Moore, A.N. (2001). Enhanced neurogenesis in the rodent hippocampus following traumatic brain injury. J. Neurosci. Res. *63*, 313–319.

Echegoyen, J., Armstrong, C., Morgan, R.J., and Soltesz, I. (2009). Single application of a CB1 receptor antagonist rapidly following head injury prevents long-term hyperexcitability in a rat model. Epilepsy Res. *85*, 123–127.

Encinas, J.M., Michurina, T.V., Peunova, N., Park, J.H., Tordo, J., Peterson, D.A., Fishell, G., Koulakov, A., and Enikolopov, G. (2011). Division-coupled astrocytic differentiation and age-related depletion of neural stem cells in the adult hippocampus. Cell Stem Cell *8*, 566–579.

Guo, D., Zeng, L., Brody, D.L., and Wong, M. (2013). Rapamycin attenuates the development of posttraumatic epilepsy in a mouse model of traumatic brain injury. PLoS One *8*, e64078.

Gupta, A., Elgammal, F.S., Proddutur, A., Shah, S., and Santhakumar, V. (2012). Decrease in tonic inhibition contributes to increase in dentate semilunar granule cell excitability after brain injury. J. Neurosci. *32*, 2523–2537.

Herman, S.T. (2002). Epilepsy after brain insult: targeting epileptogenesis. Neurology *59*, S21–S26.

Hunt, R.F., Boychuk, J.A., and Smith, B.N. (2013). Neural circuit mechanisms of post-traumatic epilepsy. Front. Cell. Neurosci. *7*, 89.

Jacob, B., and Osato, M. (2009). Stem cell exhaustion and leukemogenesis. J. Cell. Biochem. *107*, 393–399.

Kempermann, G., Song, H., and Gage, F.H. (2015). Neurogenesis in the adult hippocampus. Cold Spring Harb. Perspect. Med. *5*, a018812.

Kernie, S.G., and Parent, J.M. (2010). Forebrain neurogenesis after focal Ischemic and traumatic brain injury. Neurobiol. Dis. *37*, 267–274.

Kharatishvili, I., Nissinen, J.P., McIntosh, T.K., and Pitkanen, A. (2006). A model of posttraumatic epilepsy induced by lateral fluid-percussion brain injury in rats. Neuroscience *140*, 685–697.

Kirby, E.D., Kuwahara, A.A., Messer, R.L., and Wyss-Coray, T. (2015). Adult hippocampal neural stem and progenitor cells regulate the neurogenic niche by secreting VEGF. Proc. Natl. Acad. Sci. USA *112*, 4128–4133.

Lee, C., and Agoston, D.V. (2009). Inhibition of VEGF receptor 2 increased cell death of dentate hilar neurons after traumatic brain injury. Exp. Neurol. *220*, 400–403.

Li, Y., Korgaonkar, A.A., Swietek, B., Wang, J., Elgammal, F.S., Elkabes, S., and Santhakumar, V. (2014). Toll-like receptor 4 enhancement of non-NMDA synaptic currents increases dentate excitability after brain injury. Neurobiol. Dis. *74*, 240–253.

Louissaint, A., Jr., Rao, S., Leventhal, C., and Goldman, S.A. (2002). Coordinated interaction of neurogenesis and angiogenesis in the adult songbird brain. Neuron *34*, 945–960.

Lu, K.T., Sun, C.L., Wo, P.Y., Yen, H.H., Tang, T.H., Ng, M.C., Huang, M.L., and Yang, Y.L. (2011). Hippocampal neurogenesis after traumatic brain injury is mediated by vascular endothelial growth factor receptor-2 and the Raf/MEK/ERK cascade. J. Neurotrauma *28*, 441–450.

Marti, H.J., Bernaudin, M., Bellail, A., Schoch, H., Euler, M., Petit, E., and Risau, W. (2000). Hypoxia-induced vascular endothelial growth factor expression precedes neovascularization after cerebral ischemia. Am. J. Pathol. *156*, 965–976.

McCloskey, D.P., Croll, S.D., and Scharfman, H.E. (2005). Depression of synaptic transmission by vascular endothelial growth factor in adult rat hippocampus and evidence for increased efficacy after chronic seizures. J. Neurosci. *25*, 8889–8897.

Neuberger, E.J., Abdul-Wahab, R., Jayakumar, A., Pfister, B.J., and Santhakumar, V. (2014). Distinct effect of impact rise times on immediate and early neuropathology after brain injury in juvenile rats. J. Neurosci. Res. *92*, 1350–1361.

Parent, J.M., Yu, T.W., Leibowitz, R.T., Geschwind, D.H., Sloviter, R.S., and Lowenstein, D.H. (1997). Dentate granule cell neurogenesis is increased by seizures and contributes to aberrant network reorganization in the adult rat hippocampus. J. Neurosci. *17*, 3727–3738.

Pitkanen, A., Kemppainen, S., Ndode-Ekane, X.E., Huusko, N., Huttunen, J.K., Grohn, O., Immonen, R., Sierra, A., and Bolkvadze, T. (2014). Posttraumatic epilepsy—disease or comorbidity? Epilepsy Behav. *38*, 19–24.

Rosen, L.S. (2001). Angiogenesis inhibition in solid tumors. Cancer J. *7* (*Suppl 3*), S120–S128.

Santhakumar, V., Bender, R., Frotscher, M., Ross, S.T., Hollrigel, G.S., Toth, Z., and Soltesz, I. (2000). Granule cell hyperexcitability in the early post-traumatic rat dentate gyrus: the 'irritable mossy cell' hypothesis. J. Physiol. *524* (Pt 1), 117–134.

Segi-Nishida, E., Warner-Schmidt, J.L., and Duman, R.S. (2008). Electroconvulsive seizure and VEGF increase the proliferation of neural stem-like cells in rat hippocampus. Proc. Natl. Acad. Sci. USA *105*, 11352–11357.

Shen, Q., Goderie, S.K., Jin, L., Karanth, N., Sun, Y., Abramova, N., Vincent, P., Pumiglia, K., and Temple, S. (2004). Endothelial cells stimulate self-renewal and expand neurogenesis of neural stem cells. Science *304*, 1338–1340.

Shore, P.M., Jackson, E.K., Wisniewski, S.R., Clark, R.S., Adelson, P.D., and Kochanek, P.M. (2004). Vascular endothelial growth factor is increased in cerebrospinal fluid after traumatic brain injury in infants and children. Neurosurgery *54*, 605–611, discussion 611–2.

Sierra, A., Martin-Suarez, S., Valcarcel-Martin, R., Pascual-Brazo, J., Aelvoet, S.A., Abiega, O., Deudero, J.J., Brewster, A.L., Bernales, I., Anderson, A.E., et al. (2015). Neuronal hyperactivity accelerates depletion of neural stem cells and impairs hippocampal neurogenesis. Cell Stem Cell *16*, 488–503.

Sun, D. (2014). The potential of endogenous neurogenesis for brain repair and regeneration following traumatic brain injury. Neural Regen. Res. *9*, 688–692.

Sun, D., McGinn, M.J., Zhou, Z., Harvey, H.B., Bullock, M.R., and Colello, R.J. (2007). Anatomical integration of newly generated dentate granule neurons following traumatic brain injury in adult rats and its association to cognitive recovery. Exp. Neurol. *204*, 264–272.

Sun, D., Daniels, T.E., Rolfe, A., Waters, M., and Hamm, R. (2015). Inhibition of injury-induced cell proliferation in the dentate gyrus of the hippocampus impairs spontaneous cognitive recovery after traumatic brain injury. J. Neurotrauma *32*, 495–505.

Sun, G.C., and Ma, Y.Y. (2013). Vascular endothelial growth factor modulates voltage-gated Na(+) channel properties and depresses action potential firing in cultured rat hippocampal neurons. Biol. Pharm. Bull. *36*, 548–555.

Toth, Z., Hollrigel, G.S., Gorcs, T., and Soltesz, I. (1997). Instantaneous perturbation of dentate interneuronal networks by a pressure wave-transient delivered to the neocortex. J. Neurosci. *17*, 8106–8117.

Villasana, L.E., Kim, K.N., Westbrook, G.L., and Schnell, E. (2015). Functional integration of adult-born hippocampal neurons after traumatic brain Injury(1,2,3). eNeuro *2*. http://dx.doi.org/10.1523/ENEURO.0056-15.2015.

Walker, T.L., White, A., Black, D.M., Wallace, R.H., Sah, P., and Bartlett, P.F. (2008). Latent stem and progenitor cells in the hippocampus are activated by neural excitation. J. Neurosci. *28*, 5240–5247.

Whiting, M.D., Baranova, A.I., and Hamm, R.J.. (2006). Chapter 14. Cognitive impairment following traumatic brain injury. In Animal Models of Cognitive Impairment, E.D. Levin, and J.J. Buccafusco, eds. (Boca Raton (FL)).Available from: https://www.ncbi.nlm.nih.gov/books/NBK2521/

Winocur, G., Wojtowicz, J.M., Sekeres, M., Snyder, J.S., and Wang, S. (2006). Inhibition of neurogenesis interferes with hippocampus-dependent memory function. Hippocampus *16*, 296–304.

Yu, T.S., Zhang, G., Liebl, D.J., and Kernie, S.G. (2008). Traumatic brain injury-induced hippocampal neurogenesis requires activation of early nestin-expressing progenitors. J. Neurosci. *28*, 12901–12912.

Yu, J., Proddutur, A., Swietek, B., Elgammal, F.S., and Santhakumar, V. (2016a). Functional reduction in cannabinoid-sensitive heterotypic inhibition of dentate basket cells in epilepsy: impact on network rhythms. Cereb. Cortex *26*, 4299–4314.

Yu, T.S., Washington, P.M., and Kernie, S.G. (2016b). Injury-Induced neurogenesis: mechanisms and relevance. Neuroscientist *22*, 61–71.

Stem Cell Reports, Volume *9*

Supplemental Information

Enhanced Dentate Neurogenesis after Brain Injury Undermines Long-Term Neurogenic Potential and Promotes Seizure Susceptibility

Eric J. Neuberger, Bogumila Swietek, Lucas Corrubia, Anagha Prasanna, and Vijayalakshmi Santhakumar

Supplemental Information

Supplemental Figures

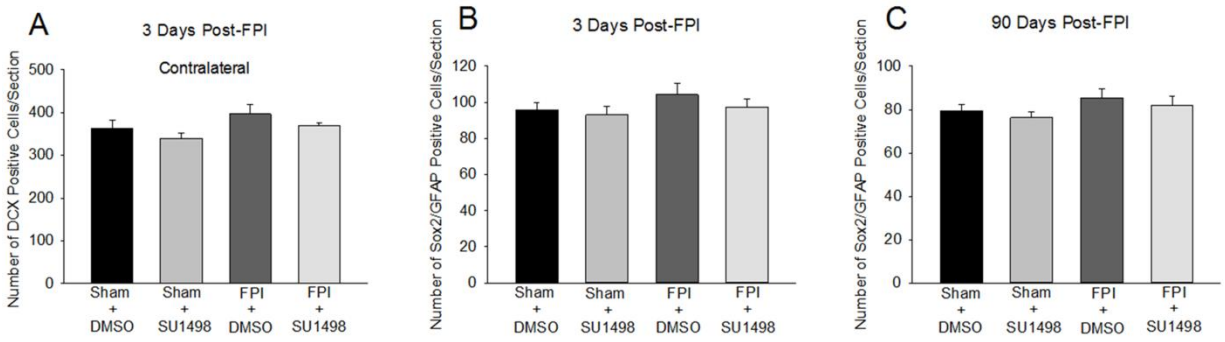

Figure S1: Effect of VEGFR2 antagonist on neurogenesis in contralateral hippocampus and Type I stem cells on the side of brain injury. (A) Stereological quantification of DCX labeled cells in contralateral sections from rats sacrificed 3 days after FPI are compared with data from age-matched sham injured controls. DCX-cells/section, sham-DMSO: 364±18, n=4 rats, sham-SU1498: 339±13, n=4 rats; FPI-DMSO: 397±23, n=4 rats, FPI-SU1498: 369±8, n=4 rats, $p>0.05$ by TW-ANOVA. There were no significant main effects on DCX cell counts as evidenced by the main effect of injury ($F_{(1, 12)} = 3.611$; $p=0.082$). and antagonist treatment ($F_{(1, 12)} = 2.494$; $p=0.140$). Interaction between injury and antagonist was also not significant ($F_{(1, 12)} = 0.00876$; $p=0.927$). (B-C) Stereological quantification of putative Type I stem cells co-labeled for Sox2 and GFAP in sections from rats sacrificed 3 (B) and 90 (C) days after FPI and compared to age-matched sham injured controls. 3 days: Sox2/GFAP-cells/section, sham-DMSO: 96±4, n=4 rats, sham-SU1498: 93±4, n=4 rats; FPI-DMSO: 104±7, n=4 rats, FPI-SU1498: 97±5, n=4 rats, $p>0.05$ by TW-ANOVA. 90 days: Sox2/GFAP-cells/section, sham-DMSO: 79±3, n=4 rats, sham-SU1498: 76±3, n=4 rats; FPI-DMSO: 85±4, n=4 rats, FPI-SU1498: 82±4, n=4 rats, $p>0.05$ by TW-ANOVA. There were no significant main effects on the total number of co-labeled cells as evidenced by the main effect of injury ($F_{(1, 12)} = 1.530$; $p=0.240$). and antagonist treatment ($F_{(1, 12)} = 0.948$; $p=0.350$). Interaction between injury and antagonist was also not significant ($F_{(1, 12)} = 0.179$; $p=0.680$). Data are shown as mean±SEM.

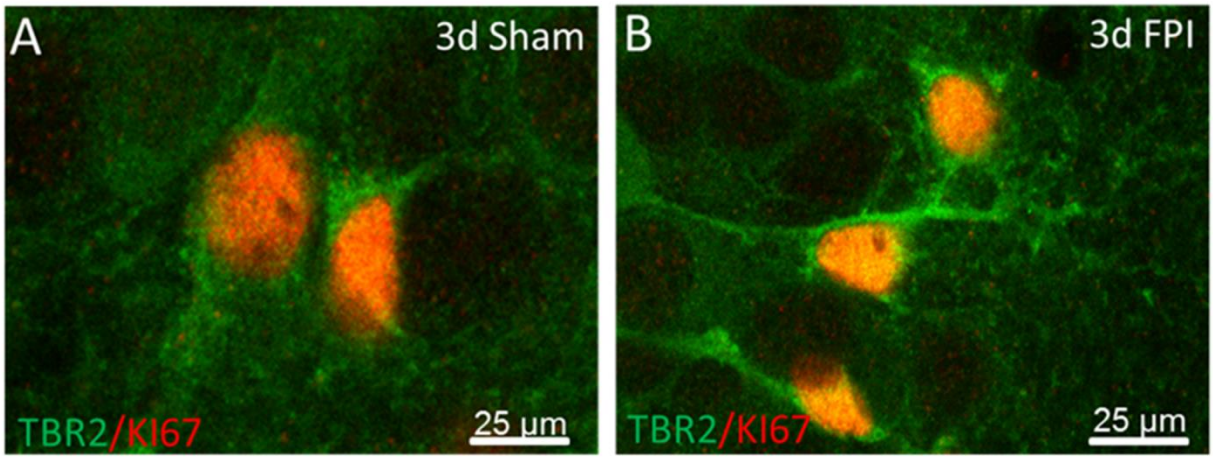

Figure S2: NPC Proliferation 3 days post-TBI

60x high magnification confocal images of sections from rats 3 days after sham (A) or FPI (B) shows NPCs co-labeled for Tbr2 and Ki67.

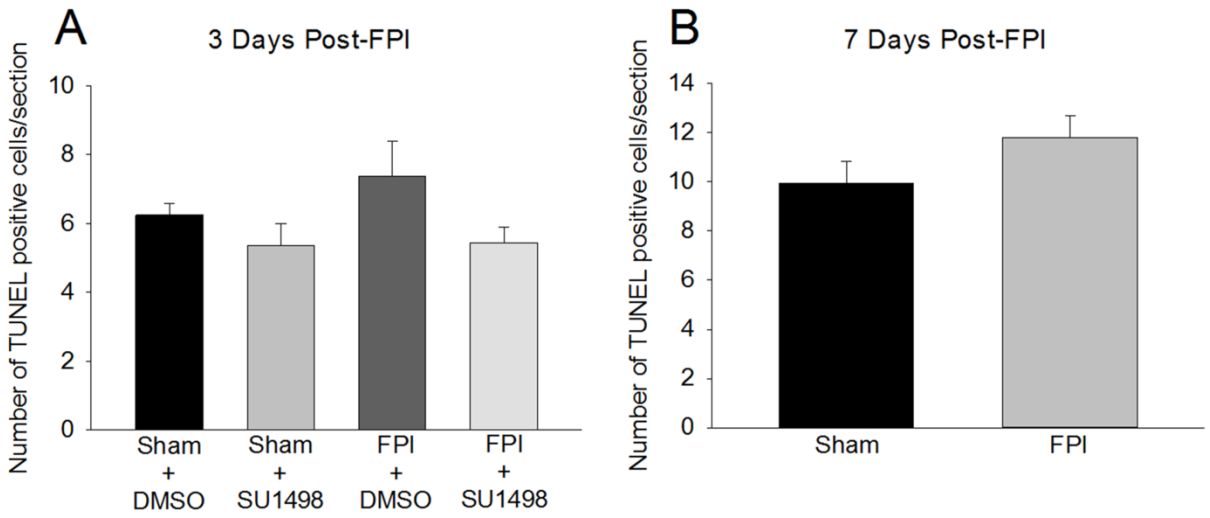

Figure S3: Lack of effect of FPI and VEGFR2 antagonist on number of TUNEL positive cells in the dentate subgranular zone. (A) Stereological quantification of TUNEL positive cells in sections from rats sacrificed 3 days after FPI are compared with data from age-matched sham injured controls. TUNEL-cells/section, sham-DMSO: 6±0, n=4 rats, sham-SU1498: 5±1, n=4 rats; FPI-DMSO: 7±1, n=4 rats, FPI-SU1498: 5±1, n=4 rats, $p>0.05$ by TW-ANOVA. (B) Stereological quantification of TUNEL positive cells in sections from rats sacrificed 7 days after FPI are compared with data from age-matched sham injured controls. TUNEL -cells/section, sham: 10±1, n=4 rats; FPI: 12±1, n=4 rats, $p>0.05$ by Student's t-test. Data are shown as mean±SEM.

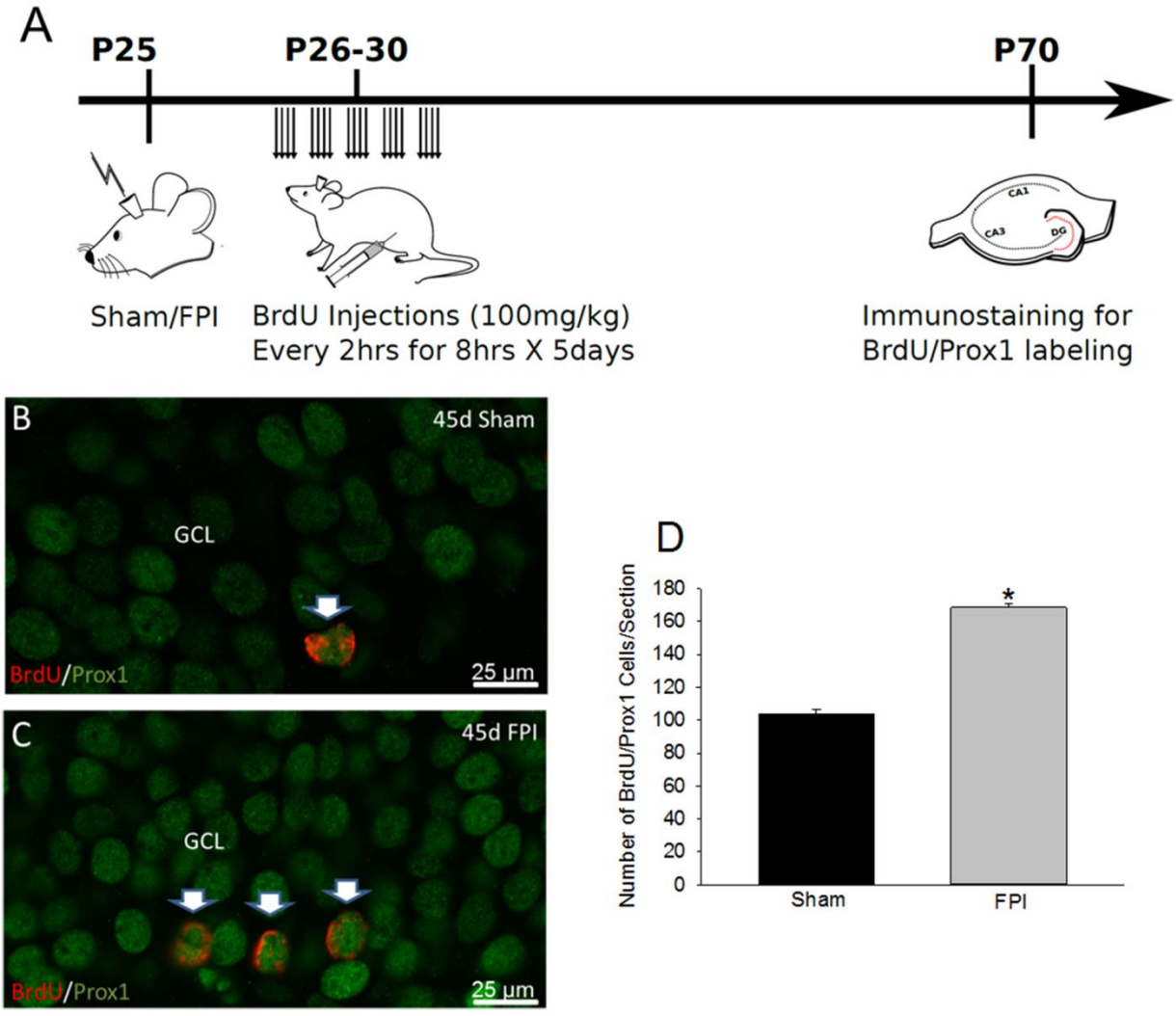

Figure S4: IGCs generated after FPI survive and mature into granule cells. (A) Schematic illustrates the timeline of FPI followed by BrdU treatment and euthanasia for histology. (B-C) Confocal images of sections from (B) control and (C) FPI rats co-labeled for BrdU and Prox1. Note the increase in neurons co-labeled for BrdU and Prox1 after FPI. (D) Summary plot shows quantification of the BrdU and Prox1 co-labeled cells 45 days after injury. BrdU/Prox-1 positive cells/section, sham: 103±3, n=4 rats, FPI: 169 ±3, n=5 rats, * indicates $p<0.05$ by Student's t-test. Data are shown as mean±SEM.

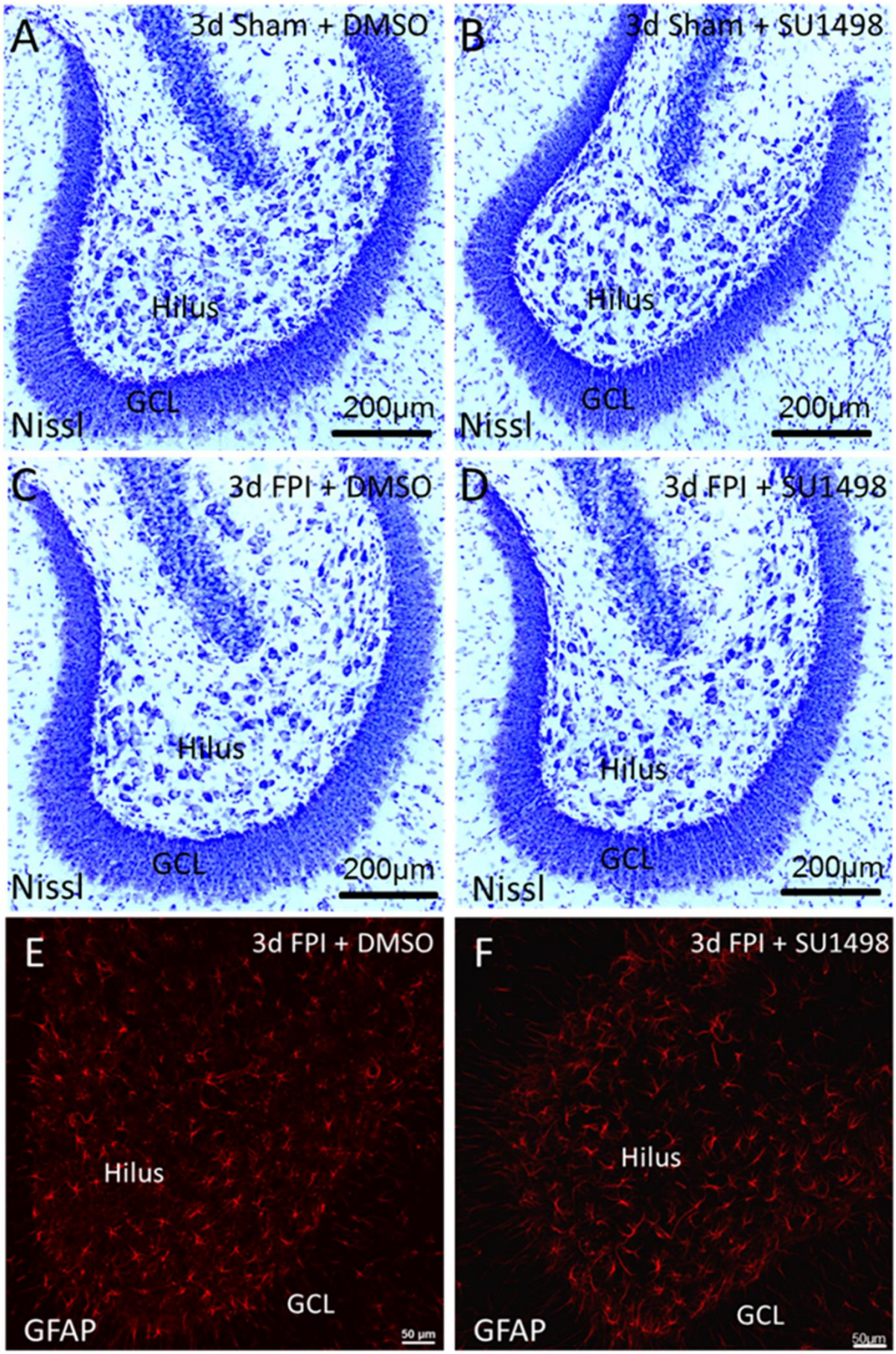
A
3d Sham + DMSO
Hilus
GCL
Nissl
200μm
B
3d Sham + SU1498
Hilus
GCL
Nissl
200μm
C
3d FPI + DMSO
Hilus
GCL
Nissl
200μm
D
3d FPI + SU1498
Hilus
GCL
Nissl
200μm
E
3d FPI + DMSO
Hilus
GCL
GFAP
50 μm
F
3d FPI + SU1498
Hilus
GCL
GFAP
50μm

Figure S5: Lack of effect of SU1498 on early post-injury hilar neuron loss and astrogliosis. (A-D) Representative Nissl stained sections from Sham and FPI rats treated with vehicle (DMSO) or SU1498 and sacrificed 3 days after injury illustrate the lack of drug effect on post-FPI hilar cell loss. N=4 sections from 4 rats for each group. (E-F) Semi-quantitative analysis of GFAP labeled cells shows application of SU1498 does not have an effect on astrocyte expression in the hippocampus 3 days after brain injury. N=6-8 sections for 4 rats for each group. Average intensity in A.U /section, FPI-DMSO: 12.02±0.58, n=4 rats; FPI-SU1498: 13.14±0.80, n=4 rats, $p>0.05$ by Student's t-test.

Supplemental Experimental Procedures

All procedures were approved by the Institutional Animal Care and Use Committee of the Rutgers New Jersey Medical School, Newark, New Jersey and are in compliance with the ARRIVE guidelines. Datasets generated during and/or analyzed during the current study are available from the corresponding author on reasonable request.

Histology and Immunohistochemistry

Immunostaining was performed on free-floating hippocampal sections (40 μm) obtained from the injured and uninjured hemisphere of FPI and age-matched sham-operated rats perfused with 4% paraformaldehyde in phosphate buffered saline 3 or 90 days after injury. Sections were washed in buffer and blocked in 10% normal donkey serum with 0.3% Triton for 1 h. For doublecortin (DCX) staining, contralateral sections were incubated overnight in anti-doublecortin primary antibody (1:100, goat polyclonal; Santa Cruz, sc-8066) in 0.3% Triton and 2% normal donkey serum. Double staining for Sox2 and GFAP was performed by sequential labeling with anti-Sox2 (1:100 goat polyclonal, Santa Cruz, sc-17320) for 1 h followed by addition of anti-GFAP (1:500, mouse monoclonal, Millipore Sigma, MAB360) and overnight incubation.

To label BrdU sections underwent DNA denaturation by serial incubation in HCL and borate buffer as detailed previously[1]. Double immunostaining for BrdU and Prox-1 was performed by sequential incubation in anti-BrdU (1:200 rat monoclonal, Abcam, AB6326) for 1 h followed by addition of anti-Prox-1 (1:2000, rabbit polyclonal, Millipore, ab-5475) overnight.

Following treatment with primary antibodies, sections were washed and immunostained with fluorescent secondary antibodies: donkey anti-goat Alexa 594 (1:500; ThermoScientific, A-11058) to reveal Doublecortin, donkey anti-goat Alexa-488 (1:500; ThermoScientific, A-11055) to reveal Sox2, donkey anti-mouse Alexa-594 (1:500; ThermoScientific, A-21203) to reveal GFAP, donkey anti-rabbit Alexa-488 (1:500; Abcam, ab150073) to reveal prox-1, donkey anti-rat Alexa-594 (1:500; ThermoScientific, A-21209) to reveal BrdU and mounted using Vectashield (Vector labs). Controls omitting primary antibody were routinely included. Fluoro-Jade C staining was performed as detailed previously [2] and positive controls were routinely included.

Quantification was performed using randomized systematic sampling protocols, selecting every tenth section along the septo-temporal axis with the hippocampus on the injured side. Cell counts were performed with the Optical Fractionator probe of Stereo Investigator V.10.02 (MBF Bioscience) at X100 (oil objective) on an Olympus BX51 microscope. In each section, the subgranular zone was outlined by a contour traced under a X10 objective (Fig. 1F) and the number of labeled cells was estimated based on planimetric volume calculations in Stereo Investigator.

Nissl Staining

Nissl staining was performed on sections from rats fixed with 4% paraformaldehyde 3 days after sham or head injury. Hippocampal sections (40 μm) were mounted on Superfrost Plus slides (Fisher Scientific – 12.550.15) and air dried. Slides were immersed in 100%, 90% 70% and 30% ethanol, and water for 30 seconds each followed by a 1 min incubation in a cresyl violet solution before being dehydrated in 30%, 70%, 90% and 100% alcohol and water for 30 seconds each and then cleared in xylene for 2 min. The sections were then mounted with DPX.

Tunel Staining

Tunel staining (Invitrogen APO-BrdU TUNEL Assay Kit – A23210) was performed on sections from rats fixed with 4% paraformaldehyde 3 days after sham or head injury. Hippocampal sections were mounted on Superfrost Plus slides (Fisher Scientific – 12.550.15), air dried and a pap pen was used to outline the sections in a hydrophobic barrier and in each step 50 uls of solution was applied to each section. First a DNA labeling solution containing a reaction buffer, TdT enzyme and BrdUTP was added to the sections and incubated at 37 degrees C for 120 minutes. Sections were then rinsed for 5 minutes and an antibody solution containing Alexa Fluor 488 dye-labeled anti BrdU antibody was applied to each section and incubated in the dark for 45 minutes. A staining buffer of propodium iodide/RNase A was then added to each section and incubated in the dark for 30 minutes. A wash buffer was then added for each section for 5 minutes for 2 consecutive washes. The sections were then air dried and mounted with Vectashield.

BrdU Labeling

For labeling neurons born after FPI, animals received four injections of 5-bromo-2-deoxyuridine (BrdU) (100 mg/kg, i.p; ThermoFisher, 000103) at two hour intervals for 5 consecutive days immediately following FPI or sham-injury[1].

References

1 Covey, M. V., Jiang, Y., Alli, V. V., Yang, Z. & Levison, S. W. Defining the critical period for neocortical neurogenesis after pediatric brain injury. *Dev Neurosci* **32**, 488-498, doi:10.1159/000321607 (2010).

2 Neuberger, E. J., Abdul-Wahab, R., Jayakumar, A., Pfister, B. J. & Santhakumar, V. Distinct effect of impact rise times on immediate and early neuropathology after brain injury in juvenile rats. *Journal of neuroscience research* (2014).